PERGAMON

International Journal of Heat and Mass Transfer 42 (1999) 3147–3158

International Journal of HEAT and MASS TRANSFER

# Turbulent heat transfer to near-critical water in a heated curved pipe under the conditions of mixed convection

L.J. Li, C.X. Lin, M.A. Ebadian*

*Hemispheric Center for Environmental Technology, Florida International University, University Park Campus, Miami, FL 33199, USA*

Received 21 May 1998; received in revised form 24 October 1998

**Abstract**

Numerical modeling was performed to investigate the developing turbulent flow and heat transfer characteristics of water near the critical point in a curved pipe. The renormalization group (RNG) $\kappa$–$\epsilon$ model was used to account for the turbulent flow and heat transfer in the curved pipe at a constant wall temperature with or without buoyancy force effect. A control volume finite element method (CVFEM) was used to solve the three-dimensional full elliptic governing equations for the problem numerically. Due to the great variation in physical properties of water near the critical point, the turbulent flow heat transfer can be significantly altered compared with the pure forced convection in the curved pipe. This study explored the influence of the near-critical pressure and wall temperature on the development of fluid flow and heat transfer along the pipe. The numerical results for forced convective flow and heat transfer were compared with experiments available in the literature. Based on the results of this research, the velocity, temperature, heat transfer coefficient, friction factor distribution, and effective viscosity are presented graphically and analyzed. 

## 1. Introduction

Turbulent flow and heat transfer to water in the region of the critical point are very complicated due to the large variation of thermal and transport properties. Fig. 1 shows the physical property variation of water at pressures slightly above the critical value according to the formulation by Lester et al. [1]. The sharp peak of specific heat capacity occurs at the so-called pseudocritical temperature, which is dependent upon pressure. The density, heat conductivity, and viscosity vary dramatically near the pseudocritical point. Density variation causes the buoyancy effect and thereby affects the flow structure and transport characteristics. In addition, the variations in properties are coupled with the flow and heat transfer. Many experimental and theoretical studies [2–5] investigated the flows of near-critical water in heated vertical and horizontal straight pipes. To the author's knowledge, there has been no research on turbulent heat transfer to near-critical water in a curved pipe, which needs to be understood because of its wide applications in power generation systems and reactor facilities.

The turbulent flow and heat transfer to the near-critical water in a curved pipe features secondary flow caused by the centrifugal force and by the buoyancy force, with dramatically varied physical properties. In general, it is more complicated than the pure convective heat transfer of fluids in the curved pipe under

* Corresponding author. Tel: +1-305-348-3585; fax: +1-305-348-4176.

*E-mail address:* ebadian@eng.fiu.edu (M.A. Ebadian)

0017-9310/99/$ - see front matter 
PII: S0017-9310(98)00365-2

**Nomenclature**

| | |
|---|---|
| $a$ | radius of the helical pipe [m] |
| $A$ | area [$m^2$] |
| $c_p$ | specific heat capacity [J ($kg^{-1}$ $K^{-1}$)] |
| $c_{\epsilon 1}$, $c_{\epsilon 2}$, $c_\mu$ | turbulent model constant |
| $d_h$ | hydraulic diameter of the helical pipe [m] |
| $D_n$ | Dean's number ($=Re \cdot \delta^{1/2}$) |
| $f_m$ | peripherally averaged friction factor [$(1/2\pi) \int_0^{2\pi} \tau_w/(\rho_{in} u_{in}^2/2)\, d\theta$] |
| $h$ | peripherally averaged heat transfer coefficient [$=(1/2\pi) \int_0^{2\pi} q_w/(T_w - T_b)\, d\theta$] |
| $k$ | turbulent kinetic energy [$m^{-2}$ $s^2$] |
| $Nu_{fd}$ | fully developed average Nusselt number |
| $Nu_m$ | peripherally averaged Nusselt number on a cross-section ($=(1/2\pi) \int_0^{2\pi} Nu_\theta\, d\theta$) |
| $Nu_\theta$ | local Nusselt number on the circumference of a pipe [$=(q_w d_h/\Gamma_l)/(T_w - T_b)$] |
| $p$, $p_c$ | pressure and critical pressure [N $m^{-2}$] |
| $p_r$ | relative pressure parameter ($=p/p_c$) |
| $Pr$ | molecular Prandtl number |
| $R_c$ | radius of the coil [m] |
| $Re$ | Reynolds number ($=\rho_{in} u_{in} d_h/\mu$) |
| $T$ | temperature [K] |
| $T_w$ | wall temperature [K] |
| $u_i$ | velocity component in $i$-direction ($i=1, 2, 3$) [m $s^{-1}$] |
| $u_{in}$ | inlet velocity [m $s^{-1}$] |
| $u_S$ | axial velocity [m] |
| $U_S$ | nondimensional axial velocity ($=u_s/u_0$) |
| $x_i$ | Cartesian coordinate in the $i$-direction ($i=1, 2, 3$) [m] |

*Greek symbols*

| | |
|---|---|
| $\alpha_T$, $\alpha_k$, $\alpha_\epsilon$ | inverse effective Prandtl number for energy equation, $k$ and $\epsilon$ |
| $\Gamma$ | thermal conductivity [W ($m^{-1}$ $K^{-1}$)] |
| $\delta$ | curvature ratio of curved pipe ($=a/R_c$) |
| $\epsilon$ | dissipation ratio of turbulent kinetic energy [$m^2$ $s^{-3}$] |
| $\theta$ | orthogonal azimuthal angle [°] |
| $\Theta$ | nondimensional temperature [$=(T - T_w)/(T_{in} - T_w)$] |
| $\mu$ | viscosity [kg ($m^{-1}$ $s^{-1}$)] |
| $\mu_{eff}$ | effective viscosity [kg ($m^{-1}$ $s^{-1}$)] |
| $\rho$ | density of fluid [kg $m^{-3}$] |
| $\tau_w$ | wall shear stress [N $m^{-2}$] |
| $\varphi$ | axial angle [°] |

*Subscripts*

| | |
|---|---|
| b | bulk quantity |
| eff | turbulent effective parameters |
| fd | fully developed situation |
| $i$, $j$, $k$ | general spatial indices |
| in | inlet conditions |
| t | turbulent quantity |
| w | wall |

normal conditions. In this study, the Computational Fluid Dynamics (CFD) software, FLUENT/UNS, was used to solve the fully elliptic governing conservation equations of the problem. The density fluctuation effect was included in the renormalization group (RNG) $\kappa$–$\epsilon$ turbulence model [6]. The computations were per-

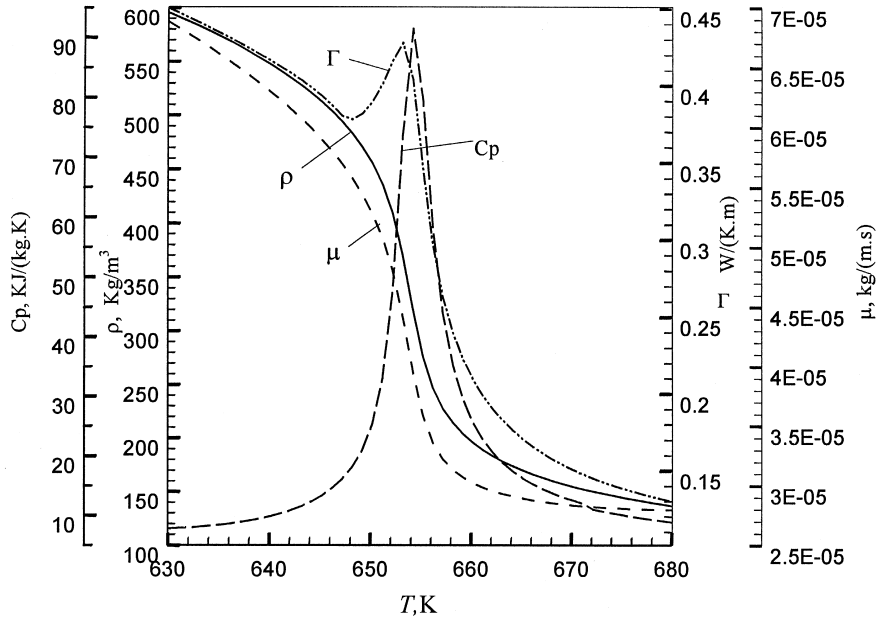


Fig. 1. Physical properties of near-critical water at $p=24$ MPa.

formed to investigate the effects of the supercritical pressure and the wall temperature on the characteristics of the mixed turbulent flow and heat transfer in a curved pipe.

## 2. Calculation models

The schematic representation of the curved pipe in both Cartesian and helical coordinate systems is shown in Fig. 2. The computation domain considered in the study was almost one complete turn of the curved pipe, with the axial angle ranging from 0–355° and with a curvature of $\delta=0.05$. Assuming that the near-critical water enters the pipe with a uniform temperature and velocity profile, and the wall was kept at constant temperature, $T_w$, the flow and thermal boundary layers developed simultaneously downstream in the curved pipe.

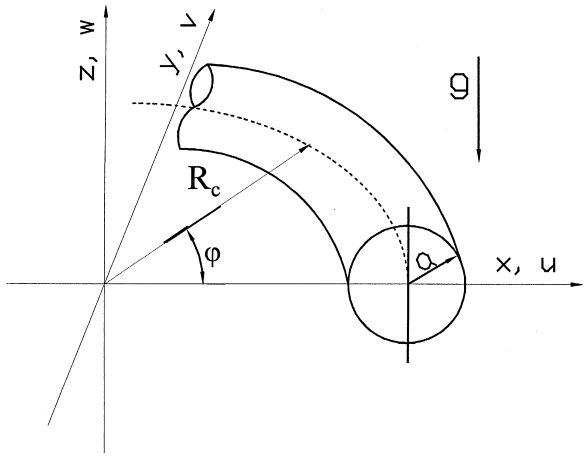


Fig. 2. Schematic of a curved pipe.

The RNG $\kappa$–$\epsilon$ model proposed by Yakhot and Orszag [6] was selected to model the turbulent flow and heat transfer in the curved pipe because the RNG model includes an additional term in its $\epsilon$ equation that significantly improves the accuracy for rapidly strained flows, such as those in curved pipes. In the present study, the near-critical water was considered as incompressible fluid. Except density, all the variable properties were taken into account in the numerical model and computation. To deal with the buoyancy effect caused directly by density difference, the Boussinesq approximation was applied in this study. The governing equations were solved in the Cartesian coordinate system in the numerical solver described later. The time-averaged, fully elliptic three-dimensional differential governing equations can be written in tensor form in the Cartesian system as follows:

Mass:

$$\frac{\partial u_i}{\partial x_i}=0. \tag{1}$$

Momentum:

$$\frac{\partial}{\partial x_j}(\rho u_i u_j) = \frac{\partial}{\partial x_j}\left[\mu_{\text{eff}}\left(\frac{\partial u_i}{\partial x_j} + \frac{\partial u_j}{\partial x_i}\right) - \frac{2}{3}\mu_{\text{eff}}\frac{\partial u_k}{\partial x_k}\right] - \frac{\partial p}{\partial x_i} + \rho g_i. \quad (2)$$

Energy:

$$\frac{\partial}{\partial x_i}(\rho u_i c_p T) = \frac{\partial}{\partial x_i}\left[\alpha_T\left(\mu_{\text{eff}}\frac{\partial T}{\partial x_i}\right)\right] + \frac{\partial u_i}{\partial x_j}\left[\mu_{\text{eff}}\left(\frac{\partial u_i}{\partial x_j} + \frac{\partial u_j}{\partial x_i}\right) - \frac{2}{3}\mu_{\text{eff}}\frac{\partial u_k}{\partial x_k}\delta_{ij}\right]. \quad (3)$$

Turbulent kinetic energy:

$$\frac{\partial}{\partial x_i}(\rho u_i k) = \frac{\partial}{\partial x_i}\left[\left(\alpha_k \mu_{\text{eff}}\frac{\partial k}{\partial x_i}\right)\right] + \mu_t S^2 + G_b - \rho\epsilon. \quad (4)$$

Dissipation rate of turbulent kinetic energy:

$$\frac{\partial}{\partial x_i}(\rho u_i \epsilon) = \frac{\partial}{\partial x_i}\left[\left(\alpha_\epsilon \mu_{\text{eff}}\frac{\partial \epsilon}{\partial x_i}\right)\right] + C_{1\epsilon}\frac{\epsilon}{k}\mu_t S^2 - C_{2\epsilon}\rho\frac{\epsilon^2}{k} - R. \quad (5)$$

The effective viscosity, $\mu_{\text{eff}}$, was calculated by the following equation:

$$\mu_{\text{eff}} = \mu_{\text{mol}}\left[1 + \sqrt{\frac{C_\mu}{\mu_{\text{mol}}}}\frac{k}{\sqrt{\epsilon}}\right]^2 \quad (6)$$

where $\mu_{\text{mol}}$ is the molecular viscosity. Eq. (6) indicates that the RNG $k$–$\epsilon$ model yields a good description of how the effective turbulent transport varies with the effective Reynolds number (or eddy scale), allowing an accurate extension of the model to low-Reynolds-number and near-wall flows [6]. The coefficients $\alpha_T$, $\alpha_k$, and $\alpha_\epsilon$ in Eqs. (3)–(5) are the inverse effect Prandtl numbers for $T$, $k$, and $\epsilon$, respectively. They were computed using the following formula:

$$\left|\frac{\alpha - 1.3929}{\alpha_0 - 1.3929}\right|^{0.6321}\left|\frac{\alpha + 2.3929}{\alpha_0 + 2.3929}\right|^{0.3679} = \frac{\mu_{\text{mol}}}{\mu_{\text{eff}}} \quad (7)$$

where $\alpha_0$ is equal to $1/Pr$, 1.0, and 1.0, for the computation of $\alpha_T$, $\alpha_k$, and $\alpha_\epsilon$, respectively. $S$ in Eqs. (4) and (5) is the modulus of the mean rate-of-strain tensor, $S_{ij}$, which is defined as:

$$S = \sqrt{2S_{ij}S_{ij}} \quad (8)$$

where $S_{ij} = \frac{1}{2}[(\partial u_i/\partial x_j) + (\partial u_j/\partial x_i)]$. $R$ in Eq. (5) was given by

$$R = \frac{C_\mu \rho \eta^3(1 - \eta/\eta_0)}{1 + \zeta\eta^3}\cdot\frac{\epsilon^2}{k} \quad (9)$$

where $\eta = S \cdot k/\epsilon$, $\eta_0 \approx 4.38$, $\zeta = 0.012$. The model constants $C_\mu$, $C_{1\epsilon}$, and $C_{2\epsilon}$ are equal to 0.085, 1.42, and 1.68, respectively. In the RNG $k$–$\epsilon$ model, the effects of buoyancy on turbulence can be accounted for through $G_b$ in Eq. (4). $G_b$ is defined as:

$$G_b = -g_i \alpha_T \mu_t \frac{1}{\rho}\frac{\partial T}{\partial x_i}\left(\frac{\partial \rho}{\partial T}\right)_p \quad (10)$$

where $\alpha_T$ is the inverse turbulent Prandtl number for energy as defined in Eq. (7). In the near-wall zone, the two-layer-based, nonequilibrium wall function was used for the near-wall treatment of flow in curved pipes. This method requires some consideration of mesh; i.e., the cell adjacent to the wall should be located to ensure that the parameter $y^+$ ($\equiv r u_\tau y/\mu$) or $y*$ ($\equiv \rho C_\mu^{1/4} k_P^{1/2} y_P/\mu$) falls into the 30–60 range. In the present study, the $y^+$ was adapted into the 30–60 range.

The nonslip boundary condition and a constant temperature were imposed on the pipe wall. At the inlet, all dependent variables were assumed to be of uniform profile in the direction normal to the inlet plane:

$$u = u_{\text{in}}, \quad T = T_{\text{in}}, \quad k = k_{\text{in}}, \quad \epsilon = \epsilon_{\text{in}}. \quad (11)$$

The inlet boundary values of $k$ and $\epsilon$ were computed from an estimated turbulence intensity, $I$, and turbulent length scale, $l$, as follows:

$$k_{\text{in}} = \frac{3}{2}(u_{\text{in}} I)^2, \quad \epsilon_{\text{in}} = C_\mu^{3/4}\frac{\kappa_{\text{in}}^{3/2}}{l}. \quad (12)$$

The initial turbulence intensity $I$, defined as $u'/u$, was equal to 5%, and the length scale $l$ was set to be $0.07 \cdot a$ in this study. This study did not address how the computed results were sensitive to the variations of the inlet $k$ and $\epsilon$.

At the outlet, the diffusion terms for all dependent variables were set to zero at the exit direction:

$$\frac{\partial \phi}{\partial n} = 0 \quad (13)$$

where symbol $\phi$ represents variables $u_i$, $T$, $k$, and $\epsilon$.

In this study, the thermodynamic and transport properties were calculated according to the program of Lester et al. [1].

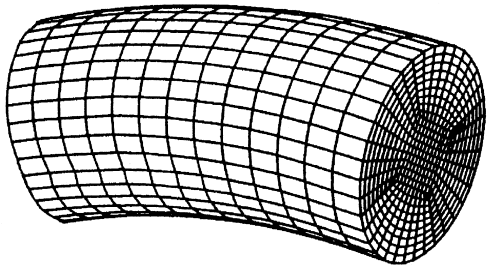

Fig. 3. Unstructured grid of the curved pipe.

## 3. Numerical computation

The turbulent mixed convective heat transfer in the curved pipe was solved by the CFD solver, FLUENT/UNS, which used a control-volume finite element method (CVFEM) similar to that introduced by Baliga and Patankar [7] to solve the governing equations. A multiblock-structured nonuniform grid system composed of hexahedral elements, schematically shown in Fig. 3, was used to discretize the computation domain.

The second-order upwind scheme proposed by Rhie and Chow [8] was selected for the discretization of the convection term in the governing equations, while the diffusion term was computed by means of multi-linear interpolating polynomials. The SIMPLEC algorithm introduced by Van Doormaal and Raithby [9] was used to resolve the coupling between velocity and pressure. Due to the large variation of the properties, the under-relaxation technique with under-relaxation factors ranging from 0.1–0.3 for all independent variables, buoyancy force term, and thermodynamic properties was adopted in the iteration procedure. The computation was considered to be converged if the following criterion was satisfied for all equations:

$$\frac{R_{\Phi}^{n}}{R_{\Phi}^{m}} \leq 10^{-4} \tag{14}$$

where $R_{\Phi}^{m}$ refers to the maximum residual value summed over all the computation cells after the $m$th (usually $m=5$) iteration and $R_{\Phi}^{n}$, the value at the $n$th iteration. To test the criterion independence, another convergence criterion of $10^{-5}$ was applied to a case. The difference of computed peripherally averaged $Nu$ numbers for the two convergence criteria was within 1%. The grid independence was investigated in the analysis by adopting different grid distributions (sectional × axial) of 320 × 120, 500 × 120, 720 × 120, 500 × 160, and 500 × 200. The grid independence test indicated that the grid system of 500 × 160 ensured a satisfactory solution. This was verified by the fact that the difference of the computed results of friction factor, temperature, and heat transfer rate with grids finer than the 500 × 160 (e.g., 500 × 200) and those with the 500 × 160 grid was within only 1%.

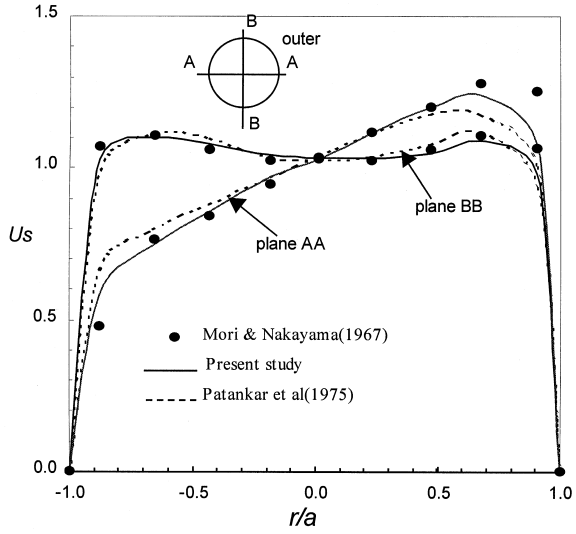


Fig. 4. Comparison of fully developed axial velocity profiles along planes AA and BB with experimental and numerical results.

## 4. Results and discussion

### 4.1. Data comparison (fully developed heat transfer)

Because there is almost no data on the turbulent mixed convective flow to near-critical water in a curved

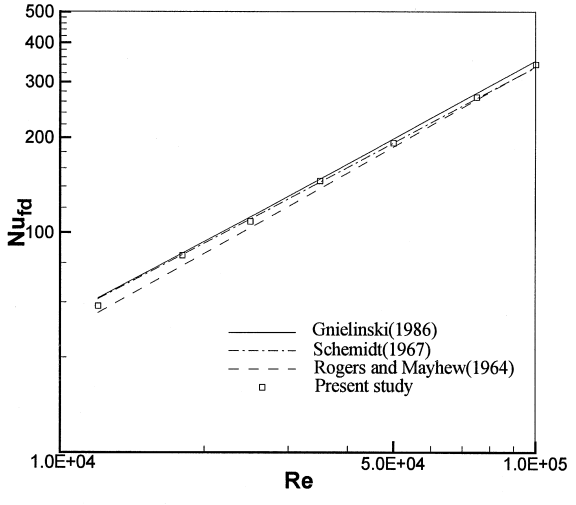


Fig. 5. Comparison of fully developed Nusselt numbers with experimental data at $\delta=0.05$, $Pr=1.293$.

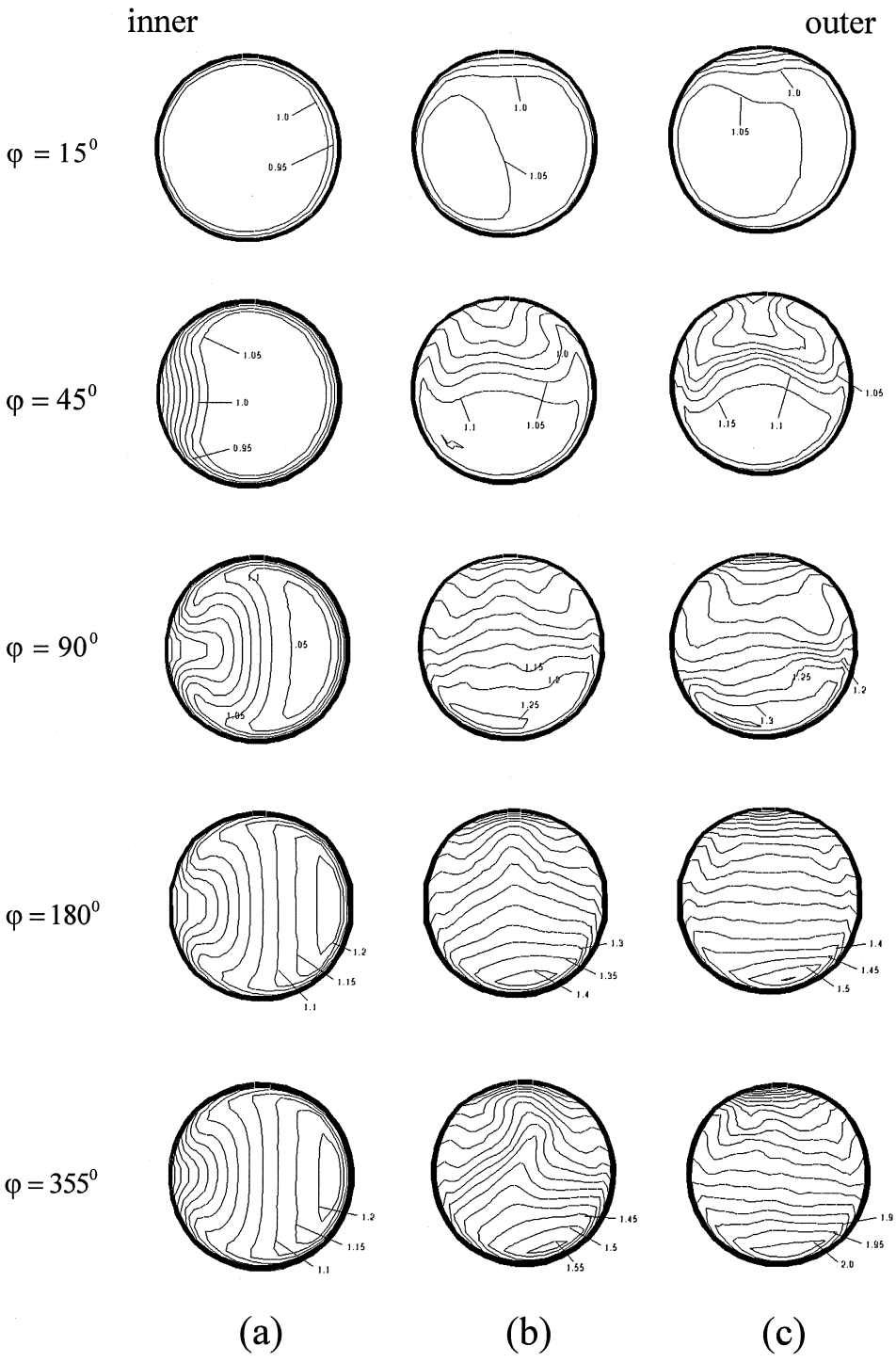


Fig. 6. Computed dimensionless isotachs at $Re = 5 \times 10^4$, $\delta = 0.05$, $T_{in} = 635$ K, $T_w = 675$ K for (a) pure convection; (b) $p = 28$ MPa; (c) $p = 23$ MPa.

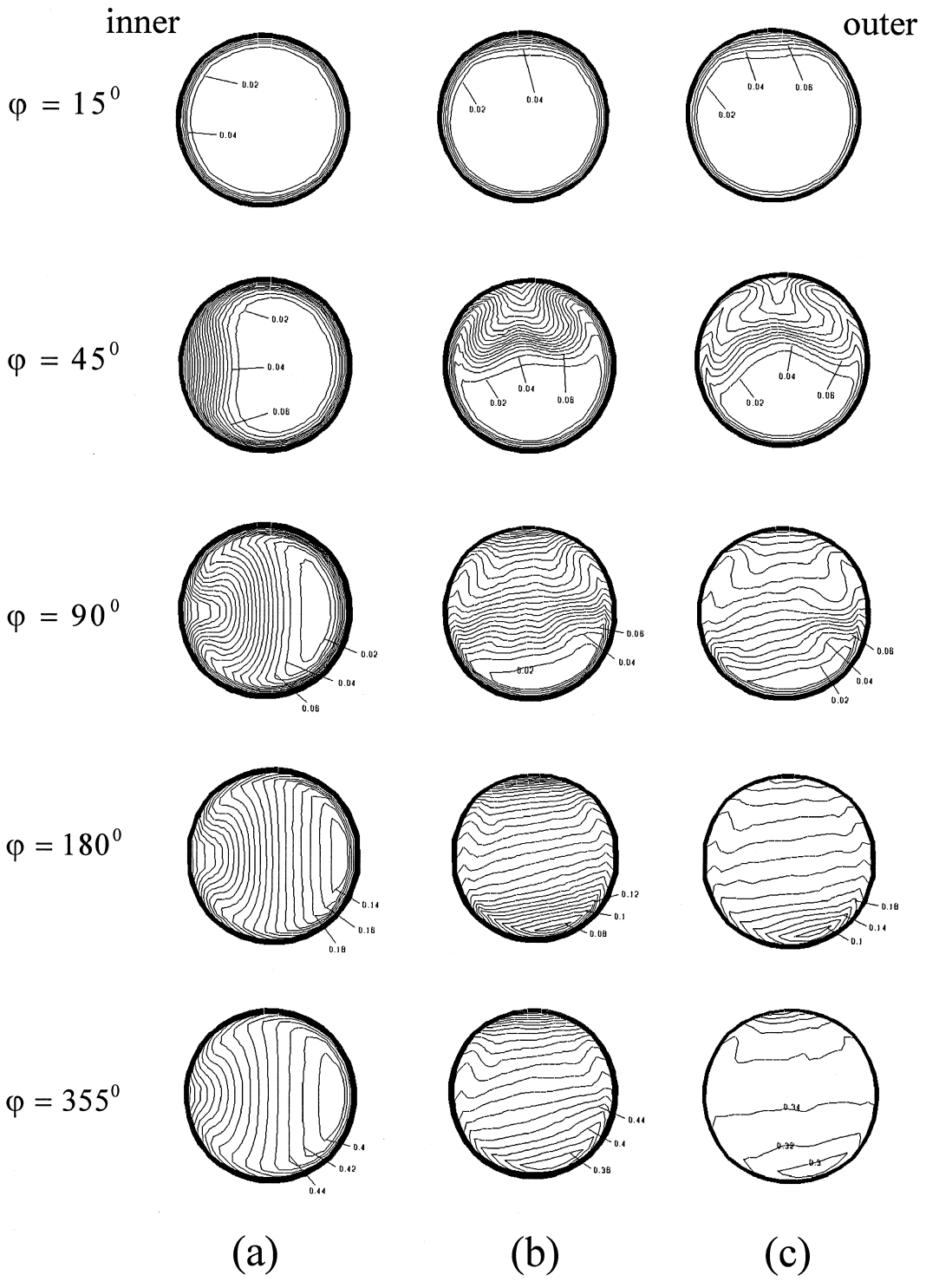


Fig. 7. Computed dimensionless isotherms at $Re = 5 \times 10^4$, $\delta = 0.05$, $T_{in} = 635$ K, $T_w = 675$ K for (a) pure convection; (b) $p = 28$ MPa; (c) $p = 23$ MPa.

pipe, the current computations were only compared with previous studies on fully developed flow and heat transfer in a curved pipe to evaluate the accuracy of the codes. By comparing the nondimensional velocity and temperature distribution between the axial positions $\varphi = 180^\circ$ and $\varphi = 355^\circ$, it was discovered that the forced turbulent flow and heat transfer in the curved pipe under non-near-critical conditions became almost fully developed at an axial position around $\varphi = 180^\circ$. Fig. 4 reveals the comparisons of the currently computed axial velocity profile for the fully developed turbulent convection with the experimental data by Mori and Nakayama [10] and parabolic numerical data by Patankar et al. [11].

Primarily due to the turbulence model used, the current numerical results showed better agreement with the experimental data than with the parabolic computations by Patankar et al. [11], especially in the region near the outer wall. In Fig. 4, the asymmetric results for plane BB were basically caused by the variable properties of the working media.

The peripherally averaged Nusselt numbers of the fully developed convection were also compared with the measurements by Rogers and Mayhew [12] and Schmidt [13], as shown in Fig. 5. According to their experimental data, Rogers and Mayhew [12] proposed the following correlation:

$$Nu_{\mathrm{fd}} = 0.023 Re^{0.85} \cdot Pr^{0.4} \cdot \delta^{0.1} \tag{15}$$

Schmidt's experimental data were presented by the following empirical formula:

$$\frac{Nu_{\mathrm{fd}}}{Nu_{\mathrm{s}}} = 1.0 + 3.6(1-\delta)\delta^{0.8} \tag{16}$$

where $Nu_{\mathrm{s}} = 0.023 Re^{0.8} \cdot Pr^{0.4}$. The curve drawn with the correlation proposed by Gnielinski [14] was also shown in Fig. 5, which can be presented as:

$$Nu_{\mathrm{fd}} = \frac{(f/8)\, Re \cdot Pr}{1 + 12.7\sqrt{f/8}(Pr^{2/3} - 1)} \left(\frac{Pr}{Pr_{\mathrm{w}}}\right)^{0.14}$$

$$f = [0.3164/Re^{0.25} + 0.03\delta^{0.5}]\left(\frac{\mu_{\mathrm{w}}}{\mu}\right)^{0.27}. \tag{17}$$

Within the examined parameter range, the maximum difference between the present study and the experimental data was less than 5%, indicating that the modeling employed in the study was correct.

### 4.2. Effect of pressure on the flow and thermal fields

It is commonly known that the flow in the curved pipe features secondary flow caused by the centrifugal force [17]. For near-critical water flow in a heated

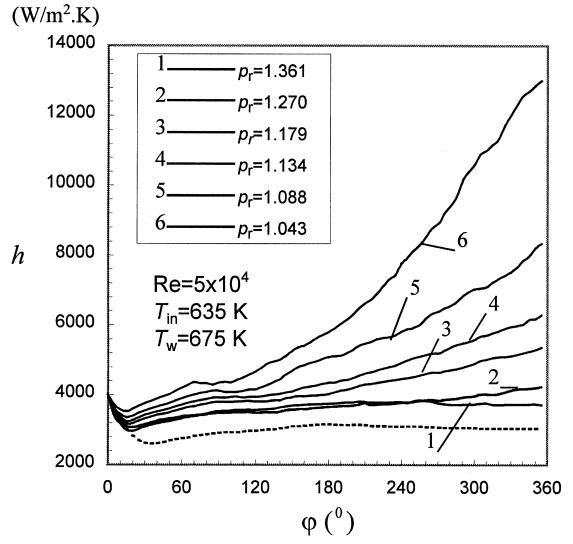


Fig. 8. Peripherally averaged heat transfer distribution along the pipe for various pressures.

curved pipe, a strong buoyancy effect is induced because of the large variation in density and the effect of other property variations. The property variation gradient for temperatures near the pseudocritical temperature is different at varied pressures, depending on the proximity of the pressure to the critical point ($p_{\mathrm{c}} = 22.05$ MPa). The closer the pressure is to the critical point, the more the properties vary with the temperatures. Fig. 6 shows the contours of the dimensionless axial velocity ($u_{\mathrm{s}}/u_{\mathrm{in}}$) at different axial positions under different pressures. The development of thermal fields is shown in Fig. 7 with contours of dimensionless isotherms. The difference in velocity magnitude between different dimensionless isotachs equals 0.05, and the difference between successive isotherms is 0.02. Figs. 6(a) and 7(a) represent the pure convection in a curved pipe without considering variations of all properties. Figs. 6(b) and 7(b) and Figs. 6(c) and 7(c) present cases in which the inlet pressures equal 28 and 23 MPa, respectively. For all cases considered here, the pseudocritical temperature at the specified pressure was higher than the inlet temperature, $T_{\mathrm{in}} = 635$ K, but lower than the wall temperature, $T_{\mathrm{w}} = 675$ K, with intent of causing large variations in the fluid properties. The Reynolds number, $Re$, for all cases at the inlet of the pipe was set to $5 \times 10^4$.

By comparing the dimensionless isotachs and isotherms at $\varphi = 180^\circ$ and $\varphi = 355^\circ$ in Figs. 6(a) and 7(a), it was evident that the pure turbulent convective heat transfer becomes almost fully developed around the axial position of $\varphi = 180^\circ$. For the turbulent flow of the near-critical fluid, due to the buoyancy effect and

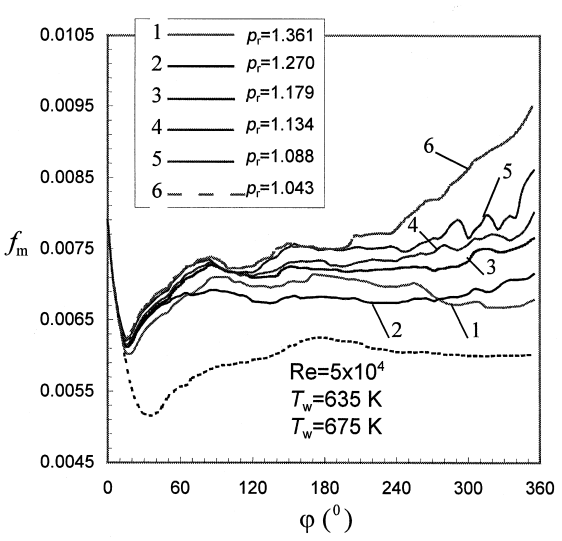


Fig. 9. Peripherally averaged friction factor distribution along the pipe for various pressures.

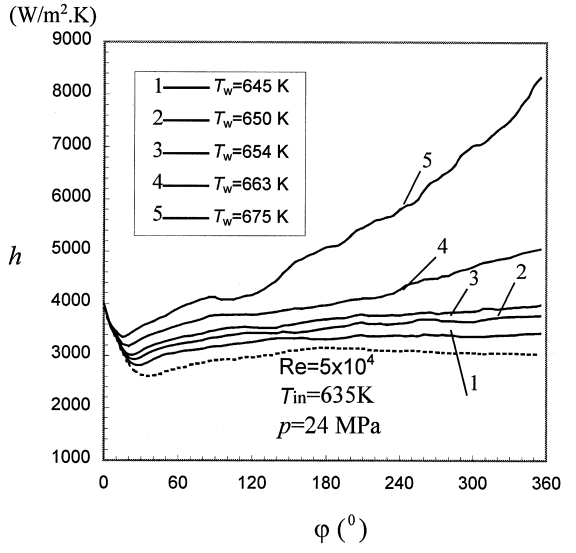


Fig. 10. Peripherally averaged heat transfer distribution along the pipe for various wall temperatures.

the variation in the transport properties, the original regular secondary flow for pure convection was altered, and the maximum velocity shifted toward the bottom of the pipe with the development of the flow fields. Under the interactive effect of the buoyancy force and the centrifugal force, the flow pattern showed sophisticated variation. For the case in which the pressure was closer to the critical point, stratification occurred for the isotachs after the axial position of $\varphi = 180^\circ$ in Fig. 6(c), indicating that the buoyancy effect was dominant over the centrifugal effect. Moreover, with the pressure nearing the critical point, the maximum and the mass-average velocities increased, but the maximum and the mass-average temperatures decreased, and the temperature in the core region tended to be comparatively uniform, which means that as pressure approached the critical point, the temperature gradient near the wall increased.

Because the thermal conductivity varied with the temperature, the Nusselt number was difficult to define. The peripherally averaged heat transfer coefficient distributions along the pipe for various pressures are shown in Fig. 8. The supercritical pressure parameter, $p_r$, varies from 1.043 to 1.361. The heat transfer coefficient distribution for pure turbulent convection is also displayed with the dashed line in Fig. 8. It was found that as pressure approached the critical point, the heat transfer coefficient was increased. This was evident especially in the second half-turn of the curved pipe. It was also found that as the flow developed downstream, the enhancement of the heat transfer was accelerated. When $p_r$ decreased 23.4% (from 1.361 to 1.043), $h$ can be increased up to 265% in the region near the outlet.

Fig. 9 shows the distribution of the peripherally averaged friction factor along the axial position at different pressures. The dashed line in Fig. 9 represents pure convection. The friction factor was based on the inlet condition, i.e., $f = \tau_w/(\rho_{in} u_{in}^2/2)$. Overall, the buoyancy effect of the supercritical water increased the

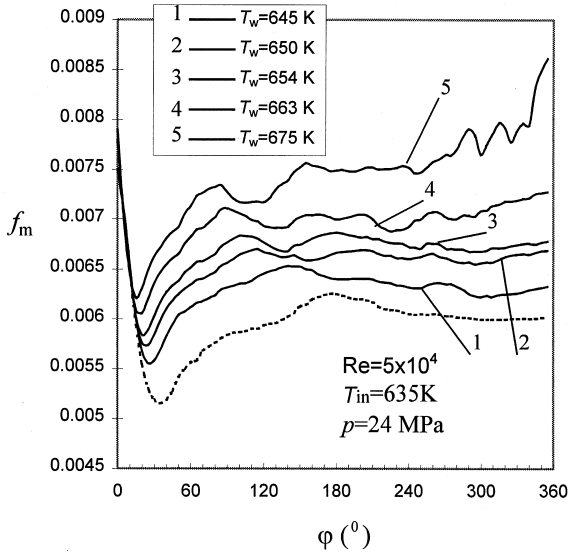


Fig. 11. Peripherally averaged friction factor distribution along the pipe for various wall temperatures.

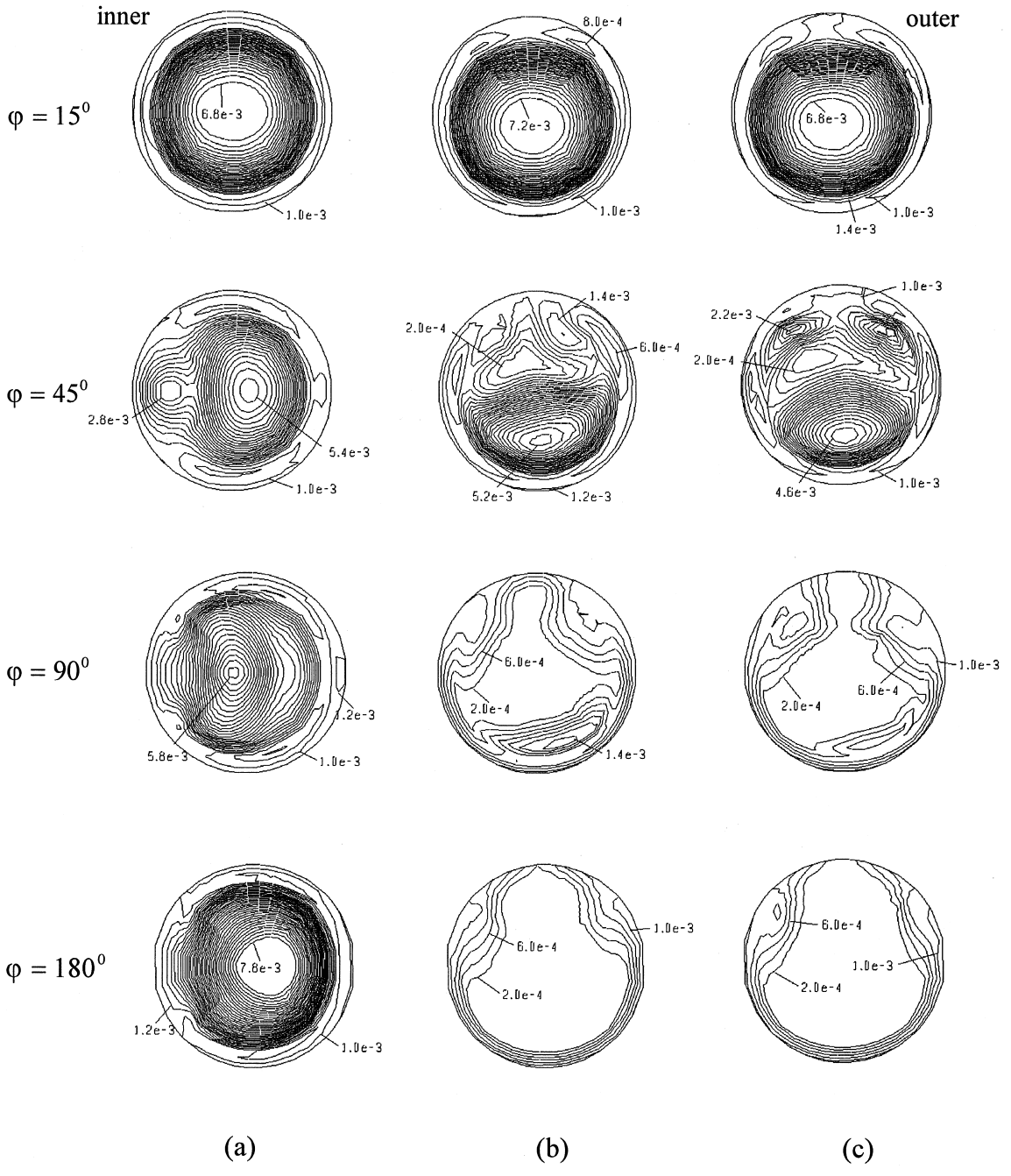


Fig. 12. Effective viscosity distribution at $Re = 5 \times 10^4$, $\delta = 0.05$ for (a) pure convection; (b) $p = 28$ MPa; (c) $p = 23$ MPa.

friction factor. The closer the pressure was to the critical point, the more the friction factor increased. Near the outlet, $f_m$ increased almost 35% when $p_r$ decreased 23.4% (from 1.361 to 1.043). The variation of $f_m$ with $p_r$ was less than that of $h$ with $p_r$ under the same conditions. Another apparent feature of the investigated flow was that the friction factor distribution showed oscillatory behavior. A similar oscillatory behavior for

the Nusselt number was also found in previous numerical studies by Patankar et al. [11], Sillekens [15], and Lin and Ebadian [16].

From the viewpoint of mechanics, the buoyancy force induced by the variable properties was in an overall direction from top to bottom at each cross-section of the pipe within the investigated parameter range of this study. The combined forced formed by the buoyancy force and the curvature-induced centrifugal force, which is in the direction from inner to outer walls, was found to be still in the direction from top to bottom (see Figs. 6 and 7). This indicated that the magnitude of the buoyancy force was always higher than the centrifugal force in this study. In general, the flow and heat transfer of the examined curved pipe were dominated by the effects of the buoyancy force.

### 4.3. Effect of wall temperature variation on the flow and heat transfer

As stated above, the density of the supercritical water varied nonlinearly with temperature near the pseudocritical temperature at a specified pressure. The density gradient with temperature had the highest value at the pseudocritical temperature. Therefore, the buoyancy force was dependent on pressure as well as temperature. Under the same inlet temperature, varying the wall temperature resulted in different buoyancy forces. The distribution of heat transfer and friction factors for various wall temperatures are shown in Figs. 10 and 11, respectively. In these figures, the dashed line denotes the pure convection for the same Reynolds number. The wall temperatures studied were set to 645, 650, 654, 633 and 675 K. Of these, the wall temperature of $T_w = 654$ K was the pseudocritical temperature for the operation pressure of $p = 24$ MPa.

For all cases in Figs. 10 and 11, both the heat transfer coefficient and the friction factor decreased along the axial position in the entrance region, reaching a minimum value at some position close to the inlet, then increased further downstream. The higher the wall temperature, the closer to the entrance was the location at which the heat transfer coefficient and the friction factor began to increase. Also, it was found in Figs. 10 and 11 that if the wall temperature was equal to or less than the pseudocritical temperature, the heat transfer coefficient and the friction factor varied slightly along the axial position after attaining their maximum values. When the wall temperature was above the pseudocritical temperature, the heat transfer coefficient increased swiftly downstream from some axial position that depended on the value of $p_r$. The point at which the heat transfer coefficient began to increase swiftly shifts closer to the inlet with the increase of the wall temperature.

### 4.4. Effective viscosity

The effective viscosity was closely related to the turbulent transport. Fig. 12 shows the distribution of the effective viscosity for pure convection and mixed convection with pressures $p = 28$ MPa and $p = 23$ MPa, an inlet temperature of $T_{in} = 635$ K, and a wall temperature of $T_w = 675$ K. The difference between successive contours equals $2 \times 10^{-4}$. In the beginning section ($\varphi \leqslant 45^\circ$), the maximum effective viscosity shifted toward the bottom of the pipe due to the buoyancy force effect, and the maximum value decreased as the pressure approached the critical point. For mixed convection downstream from $\varphi = 90^\circ$, the maximum effective viscosity moved completely to the near-wall region. This was very different from the pure convection case for which the maximum effective viscosity occurred in the core region of the curved pipe. Meanwhile, the effective viscosity in the core region became lower downstream. As a result, the effective viscosity in the thermal boundary layer near the wall decreased.

## 5. Conclusions

Three-dimensional turbulent heat transfer to near-critical water in a heated curved pipe under the conditions of mixed convection has been investigated numerically by a CVFEM. All physical and transport property variations were included in the modeling of the turbulent heat transfer.

As the pressure neared the critical point, the heat transfer coefficient and friction factor increased significantly. As the wall temperature increases above the pseudocritical temperature, the heat transfer and friction factor also increase dramatically downstream from some axial position.

The effective viscosity for turbulent mixed convection to near-critical water decreased along the curved pipe. The friction factor distribution along the pipe showed obvious oscillatory behavior.

Recommended future research on this topic includes the effects of curvature ratio on the near-critical turbulent convection and the detailed interaction between the buoyancy and centrifugal forces. Heat transfer experiments under the near-critical conditions are also desired.

## Acknowledgement

The authors gratefully acknowledge the financial support of the National Science Foundation (NSF) under Grant No. CTS-9017732.

## References


[1] H. Lester, S.G. John, S.K. George, Steam Tables, Hemisphere Publishing Co., New York, 1984.

[2] U. Renz, R. Bellinghausen, Heat transfer in a vertical pipe at supercritical pressure, in: Proceedings of the Eighth International Heat Transfer Conference, Vol. 3, 1986, pp. 957–962.

[3] A.F. Polyakov, Heat transfer under supercritical pressures, Advances in Heat Transfer 21 (1991) 1–50.

[4] V.A. Kurganov, A.G. Kaptilnyi, Flow structure and turbulent transport of a supercritical pressure fluid in a vertical heated tube under the conditions of mixed convection. Experimental data, Int. J. Heat Mass Transfer 36 (1993) 3383–3392.

[5] S. Koshizuka, N. Takano, Y. Oka, Numerical analysis of deterioration phenomena in heat transfer to supercritical water, Int. J. Heat Mass Transfer 38 (1995) 3077–3084.

[6] V. Yakhot, S.A. Orszag, Renormalization group analysis of turbulence: I. Basic theory, J. Scientific Computing 1 (1) (1986) 1–51.

[7] B.R. Baliga, S.V. Patankar, A control volume finite-element method for two-dimensional fluid and heat transfer, Numerical Heat Transfer 6 (1983) 245–261.

[8] R.M. Rhie, W.L. Chow, Numerical study of the turbulent flow past an airfoil with trailing edge separation, AIAA Journal 21 (11) (1983) 1525–1532.

[9] J.P. Van Doormaal, G.D. Raithby, Enhancements of the SIMPLE method for predicting incompressible flow problems, Numerical Heat Transfer 7 (1984) 147–158.

[10] Y. Mori, W. Nakayama, Study on forced convective heat transfer in curved pipes (2nd report, turbulent region), Int. J. Heat Mass Transfer 10 (1967) 37–59.

[11] S.V. Patankar, V.S. Pratap, D.B. Spalding, Prediction of turbulent flow in curved pipes, J. Fluid Mech. 67 (1975) 583–595.

[12] G.F.C. Rogers, Y.R. Mayhew, Heat transfer and pressure loss in helical coiled tubes with turbulent flow, Int. J. Heat Mass Transfer 7 (1964) 1207–1216.

[13] E.F. Schmidt, Warmeubergang und druckverlust in Rohrschlangen, Chemie-Ing.-Techn. 36 (1967) 781–789.

[14] V. Gnielinski, Heat transfer and pressure drop in helically coiled tubes, in: Proceedings of the Eighth International Heat Transfer Conference, Vol. 6, Tayler and Francis, Washington, DC, 1986, pp. 2847–2854.

[15] J.J.M. Sillekens, Laminar mixed convection in ducts, Ph.D. Thesis, Technische Universiteit Eindhoven, Eindhoven, 1995.

[16] C.X. Lin, M.A. Ebadian, Developing turbulent convective heat transfer in helical pipes, Int. J. Heat Mass Transfer 40 (1997) 3861–3873.

[17] S.A. Berger, L. Talbot, L.S. Yao, Flow in curved pipes, Ann. Rev. Fluid Mech. 15 (1983) 461–512.